ISSN 1063-7710, Acoustical Physics, 2011, Vol. 57, No. 3, pp. 411–419. © Pleiades Publishing, Ltd., 2011.

OCEAN ACOUSTICICS.
UNDERWATER ACOUSTICS

An Alternative Approach for Measuring the Scattered Acoustic Pressure Field of Immersed Single and Multiple Cylinders[1]

Sina Sodagar[a], Farhang Honarvar[a, b], Amin Yaghootian[a], and Anthony N. Sinclair[b]

[a] *NDE Lab., Faculty of Mechanical Engineering, K.N. Toosi University of Technology, Tehran, Iran*

[b] *Department of Mechanical and Industrial Engineering, University of Toronto, Toronto, Canada*

e-mail: honarvar@mie.utoronto.ca

Received August 27, 2010

Abstract—The form function of an elastic target can be obtained from the scattered signal through a deconvolution process. The deconvolution process uses the signal measured from an acoustically hard target (reference signal) to compensate for the impulse response of the measurement system. In this paper, it is shown that this approach limits the usable frequency range of the signal and leads to inaccuracies in the final results. An alternative approach is proposed in which the reference signal is replaced by the specular echo. A procedure is described for extracting the specular echo from the measured signal even in cases where it is not completely isolated from the resonant components. Modifications are made to the existing deconvolution formulation and it is further extended to be applicable to multiple scattering measurements. Experimental results show that the new approach provides improved accuracy and wider usable frequency range in both single and multiple scattering experiments.

DOI: 10.1134/S1063771011030201

1. INTRODUCTION

Resonance Scattering Theory (**RST**) shows that the backscattered amplitude spectrum of an elastic scatterer is a combination of resonant components superimposed on a smooth background [1–4]. It also provides mathematical tools for separating these two components. Resonance Acoustic Spectroscopy (**RAS**), which is an outcome of RST, focuses on the resonance effects present in acoustic echoes of an elastic target when the target is excited by an incident acoustic wave. For many years, RAS and other acoustic scattering techniques have been used for remote classification of submerged targets. In recent years, this technique has also been utilized for material characterization and nondestructive evaluation purposes [5, 6].

Together with theoretical developments of RST and RAS, experimental aspects of these processes have also been considered by many researchers. Maze et al. [7] presented the first experimental quasi-line spectrum obtained by the Method of Isolation and Identification of Resonances (**MIIR**) [8]. MIIR provides experimental verification and illustration of RST. Although tone bursts of long duration were used in early MIIR studies, it was later shown that short-pulse MIIR is less time consuming and more convenient [9].

Since the introduction of RST and its corresponding experimental techniques, many researchers have used them to study various aspects of wave scattering. Maze and Ripoche [10] discussed the use of MIIR for RAS of elastic objects. Brill et al. [11, 12] used RAS for characterization of the geometry of fluid scatterers. Honarvar and Sinclair [13, 14] used the short-pulse MIIR to measure the scattered pressure field of long solid elastic clad rods at both normal and oblique incident angles and showed the potential of RAS for the purpose of nondestructive evaluation (**NDE**) of cylindrical components. Mathieu et al. [15] used the backscattered echo received from a wire target to evaluate its size. Scipioni et al. [16] used two different methods for estimating the diameter of a metallic wire based on RAS.

Besides studies based on scattering from individual targets, researchers have also been interested in multiple scattering from a group of targets. An experimental study of the *A*-wave was conducted by Kheddioui et al., where two identical immersed shells were insonified by an acoustic wave in an eclipsed configuration [17]. *A*-waves are circumferential surface waves propagating in the surrounding medium around an immersed cylindrical shell. Lethuillier et al. studied the resonance scattering by two elastic cylindrical shells immersed in water [18]. Their study included both theoretical analysis and experimental measurements. Later, they conducted experimental and theoretical studies on acoustic wave scattering from a finite linear grating of elastic cylindrical shells [19].

The aim of this paper is to introduce an alternative approach to conduct short pulse MIIR measurements. In the short pulse MIIR technique, a reference signal

[1] The article is published in its original form.

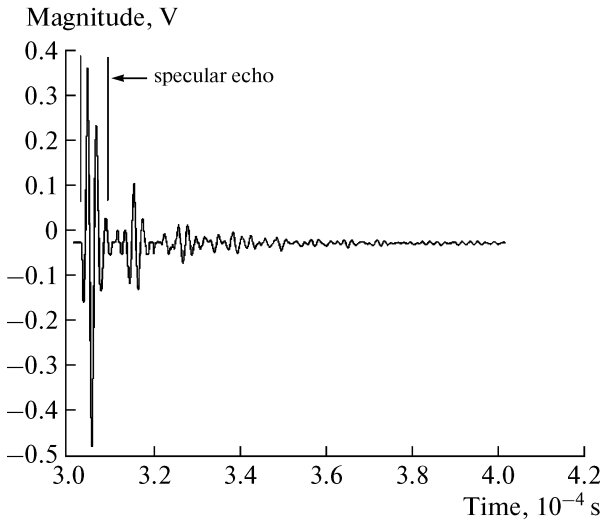

Fig. 1. Backscattered echo from a copper cylinder immersed in water [23].

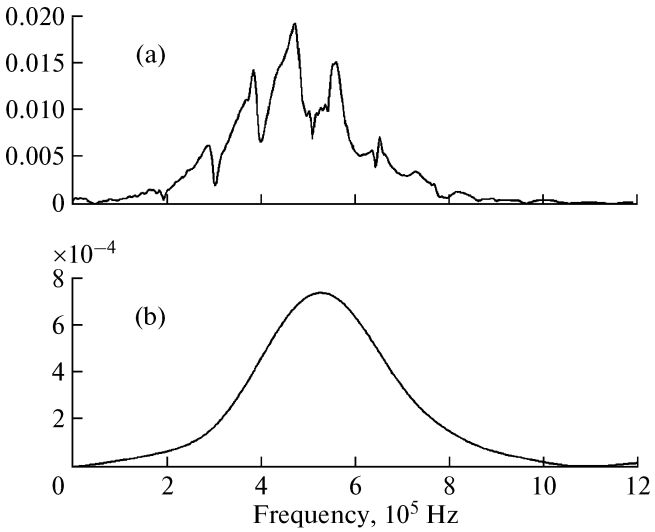

Fig. 2. Frequency spectra of the (a) backscattered echo of the copper rod, and (b) backscattered echo of a tungsten fiber [23].

is used to compensate for the impulse response of the measurement system. This reference signal is usually obtained from an acoustically hard target such as a tungsten fiber. We show that by using such a reference target, the accuracy of the measurements is reduced and limitations are imposed on the usable range of the frequency spectrum. The proposed approach does not suffer from these limitations.

2. SINGLE SCATTERING EXPERIMENTS

2.1. Short Pulse MIIR Method

In the short-pulse MIIR technique, the scatterer is insonified by short, broadband pulses. A typical echo backscattered from a copper rod is shown in Fig. 1. The first backscattered echo of the pulse returning back to the receiver corresponds to the specular reflection. The subsequent echoes are due to resonances generated by surface and subsurface waves encircling the body of the scatterer and producing leaky standing waves. The frequency spectrum of the backscattered echo is a convolution of the wave scattered from the cylinder and the impulse response of the measurement system. By compensating for the impulse response of the measurement system, and plotting the resulting spectrum as a function of the normalized frequency, ka, the form function $|f_\infty|$, of the cylinder is obtained.

The processing scheme consists of two parts: (a) measuring the frequency spectrum of the backscattered wave (see Fig. 2a), and (b) removing the frequency characteristics of the measurement system. This process is currently carried out by removing the frequency characteristics of the transducer and system electronics by a deconvolution technique which uses a reference frequency spectrum that is free from resonances; see Fig. 2b [20–24]. For this purpose, a small diameter cylindrical component of a material with high stiffness, such as tungsten, is used for producing a reference spectrum. At low ka values, none of the resonance frequencies of the tungsten fiber are excited and its frequency spectrum is smooth, see Fig. 2b. The experimental form function can then be obtained from the following equation [24]:

$$|f_\infty| = \left(\frac{S(\omega)}{S'(\omega)}\right)\left|\frac{a'}{a}\right|^{1/2}|f'_\infty|, \qquad (1)$$

where $S(\omega)$ is the frequency spectrum of the specimen, $S'(\omega)$ is the frequency spectrum of the tungsten fiber, $|f'_\infty|$ is the form function of the tungsten fiber, and a and a' are diameters of the sample rod and tungsten fiber, respectively. In Eq. (1), $S(\omega)$ and $S'(\omega)$ are experimentally measured and $|f'_\infty|$ is numerically calculated.

2.2. Effect of Target Diameter

The desired frequency range of the form function should be small enough so that none of the resonance frequencies of the tungsten fiber appear. In Fig. 3, it can be seen that in order not to have any of the resonances of the tungsten fiber excited, all measurements should be performed in the frequency range of $0 < ka < 4$, as designated by a thick solid line. This restriction forces the use of a thin tungsten fiber and a transducer with a relatively low frequency. For example, for a 500 kHz ultrasonic transducer having a useful bandwidth of 200–800 kHz, the diameter of the tungsten fiber should be less than 1.17 mm. This is usually quite different from the diameter of the test

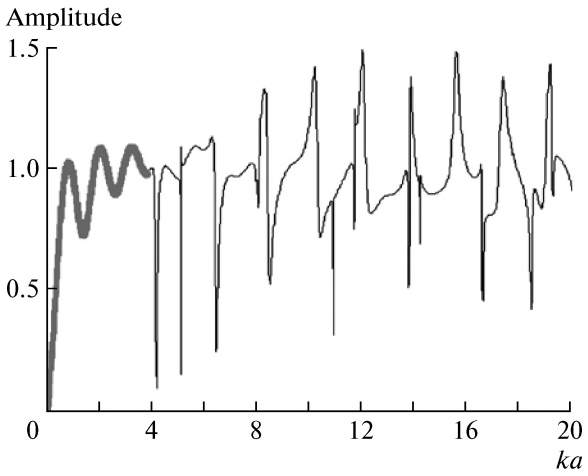

Fig. 3. Numerical form function of a tungsten fiber.

sample which is typically at least several millimeters. This difference in diameters of the specimen and reference sample could have significant effect on the final results. To investigate the effects of this difference, we measure the backscattered echo from three steel rods with different diameters. These rods have diameters of 0.38 mm, 1.60 mm and 6.34 mm and are tested by a 500 kHz immersion ultrasonic transducer.

The frequency spectra of the three rods are shown in Fig. 4 and the center frequencies and maximum amplitudes of their spectra are listed in Table 1. According to Table 1, as the diameter increases, the center frequency of the spectrum decreases while its corresponding maximum amplitude increases. Therefore, the center frequencies of the signals obtained from a small diameter tungsten fiber and the large diameter sample could be quite different. Increase in the maximum amplitude of the spectrum could be attributed to the larger reflecting surface of the thicker rods. Moreover, since high frequency components are more attenuative, it is speculated that with the increase of the diameter of the rod, the center frequency of the signal would decrease [25, 26]. Consequently, one would have different frequency spectra for the thick and thin rods.

When there exists a significant difference between diameters of the sample and reference target (tungsten fiber), the signals reflected back from them have different center frequencies and amplitudes. This difference will not lead to accurate results when these signals are implemented in the deconvolution process of Eq. (1). To demonstrate this, experiments conducted in [13] are repeated here. Figures 5a and 5b show the frequency spectra of a 0.25 mm diameter tungsten fiber and an 18.30 mm diameter copper-clad aluminum rod, respectively. Considerable difference is observed in both the center frequency and maximum amplitudes of the two frequency spectra. The ultrasonic transducer used has a bandwidth of 200–

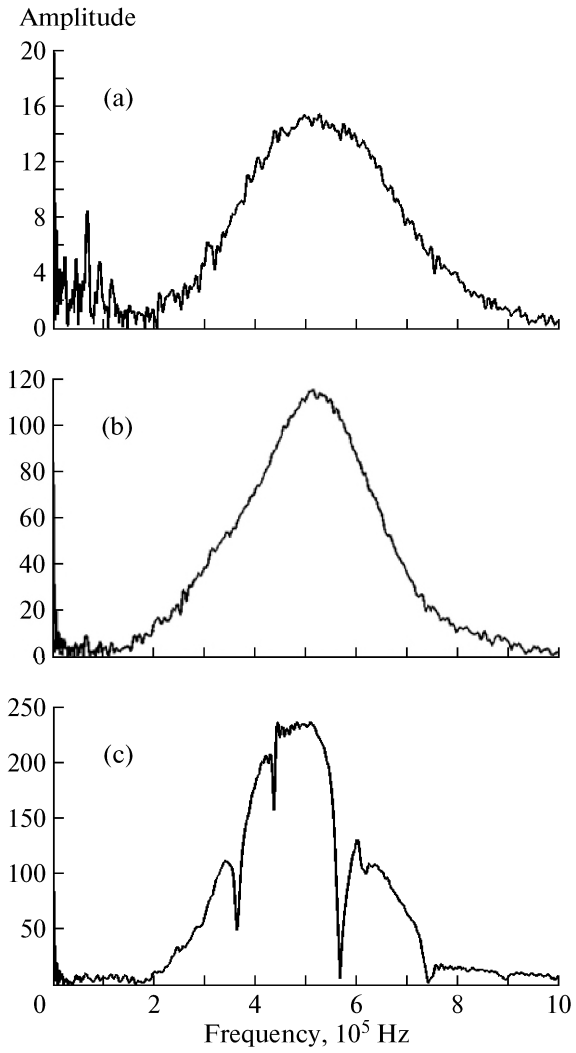

Fig. 4. Frequency spectra of the scattered echo from (a) 0.38 mm diameter steel rod, (b) 1.6 mm diameter steel rod, (c) 6.34 mm diameter steel rod obtained by a 500 kHz transducer.

800 kHz, and therefore, it is expected that the experimental results would be valid within the range of $8 < ka < 31$. By comparing the experimental form function of Fig. 6a with its corresponding calculated form function shown in Fig. 6b, we observe that the experimental and numerical results only match in the frequency range of $10 < ka < 20$. Moreover, in Fig. 6a

Table 1. Centre frequencies and maximum amplitudes of the frequency spectra of the signals scattered from different steel rods

Rod diameter, mm	Center frequency, kHz	Max. normalized amplitude
0.38	5.25	15
1.60	5.18	116
6.34	4.80	237

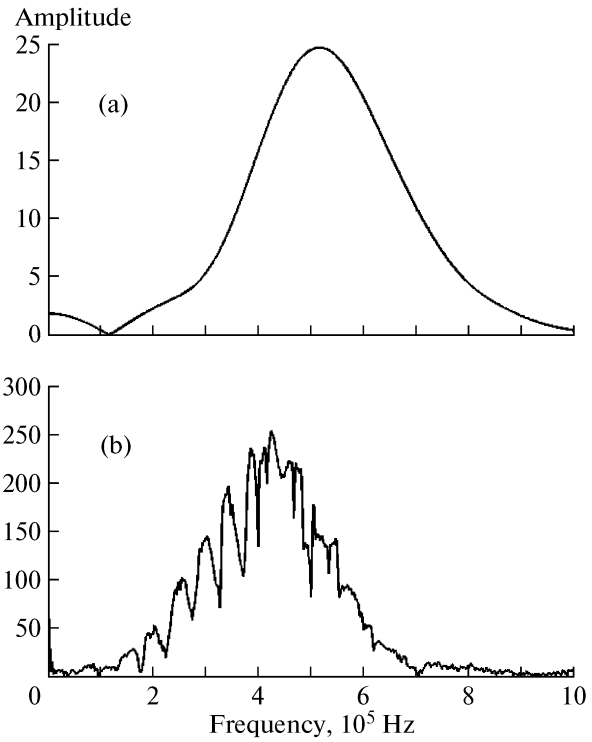

Fig. 5. (a) Frequency spectrum of the backscattered echo from a 0.25 mm diameter tungsten fiber, and (b) the backscattered echo from an 18.30 mm diameter copper-clad aluminum rod obtained by a 500 kHz transducer.

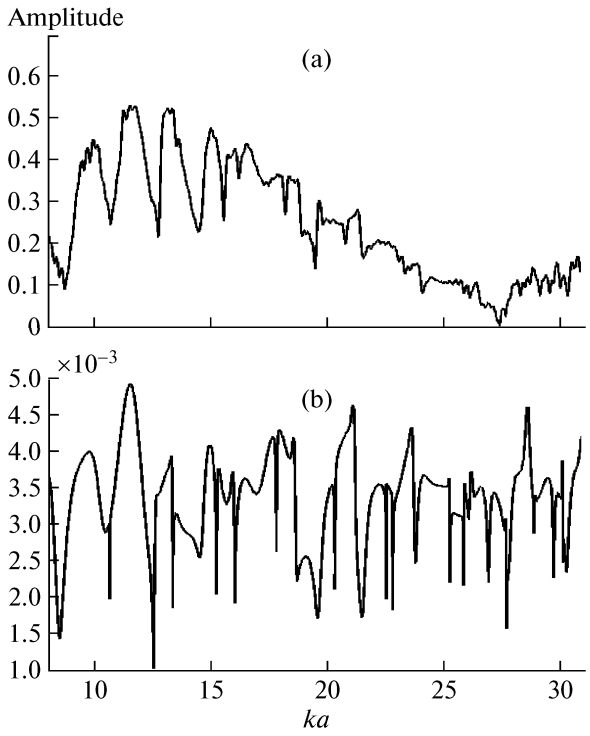

Fig. 6. (a) Experimental and (b) numerical form functions of the copper-clad aluminum rod for the frequency range of $8 < ka < 31$.

the measured form function shows a descending pattern as the normalized frequency ka increases. Although, the $(a'/a)^{1/2}$ term in Eq. (1) is supposed to compensate for the difference in diameters of the two targets, noticeable difference can still be seen in maximum amplitudes of experimental and numerical spectra in Figs. 6a and 6b.

2.3. Alternative Approach

In any backscattering measurement, the first echo in the backscattered pulse is the specular reflection corresponding to reflection from a rigid target. Echoes pertaining to resonance effects follow this echo. If the specular echo could be isolated from the rest of the signal, it can then be used as the reference signal for deconvolution purposes. In most cases this isolation is very difficult if not impossible. In what follows, we propose a technique for extracting this echo from the backscattered signal even if it is overlapping with resonance echoes.

The isolation of the specular echo can be done either during the measurement process or through post-processing. During the measurement process, this could be done by using a digital oscilloscope that could simultaneously show the acquired signal and its corresponding spectrum. We start with a signal that only includes part of the specular echo. By gradual increase of the horizontal range, we monitor the frequency spectrum of the echo and decide where the signal produces a smooth frequency spectrum. This part of the signal is then saved as the reference signal.

Alternatively, during the post-processing phase, a computer code can gradually reduce the number of data points considered in the time-domain signal until the corresponding spectrum becomes very smooth (no resonances present). The resulting signal would then correspond to the reference echo. As an example, the frequency spectra of the received signal from the copper-clad aluminum rod and its corresponding specular reflection are plotted in Fig. 7. Comparing Fig. 7 with Fig. 5, we observe that in Fig. 7, the two spectra match very well except for the resonance frequencies. However, significant differences are observed in both the amplitudes and peak frequencies of the spectra shown in Figs. 5a and 5b.

To use the specular echo as the reference signal, some modification needs to be performed to Eq. (1). The form function of the tungsten fiber, $|f'_\infty|$, should be replaced with the form function of the specular echo. Since the frequency spectrum of the specular

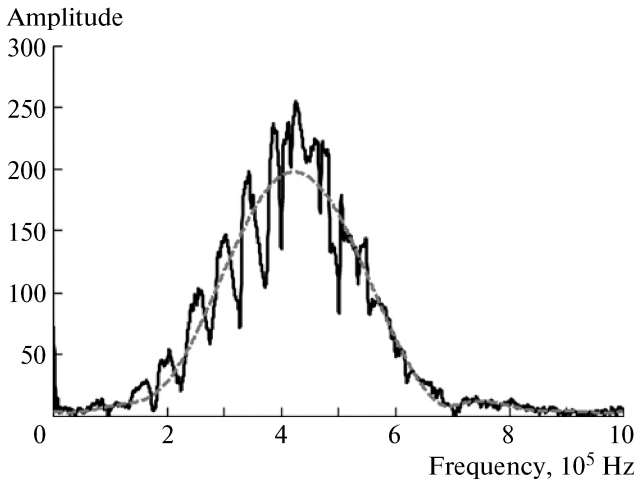

Fig. 7. Frequency spectra of the copper clad-aluminum rod (solid line) and its corresponding specular reflection (dashed line).

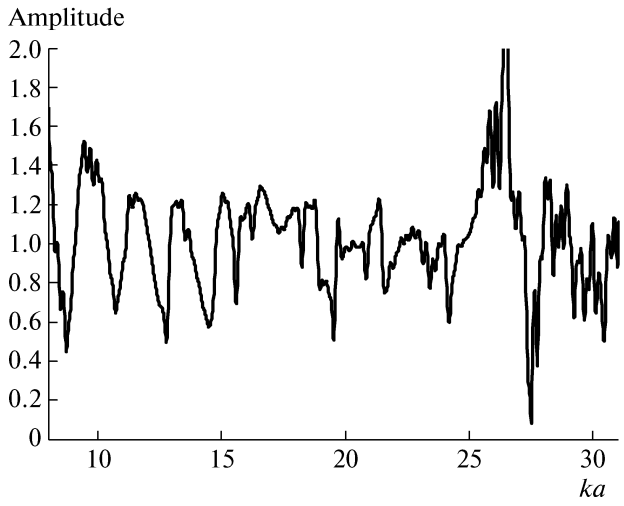

Fig. 8. Experimental form function of the copper-clad aluminum rod obtained by using the specular echo as the reference signal.

echo corresponds to the form function of a rigid cylinder, we have [1]:

$$f'_\infty = f^R_\infty = \frac{2}{\sqrt{\pi i k a}} \sum_{n=0}^{\infty} \varepsilon_n A_n(ka) \cos n\phi, \qquad (2)$$

where ε_n is the Neumann factor ($\varepsilon_n = 1$ for $n = 0$, and $\varepsilon_n = 2$ for $n > 0$), ϕ is the receiving angle, and A_n are constant coefficients obtained from:

$$A_n = -\frac{J'_n(ka)}{H_n^{(1)'}(ka)}. \qquad (3)$$

Substitution of Eq. (2) into Eq. (1) gives,

$$|f_\infty| = \left|\frac{S(\omega)}{S'(\omega)}\right| |f^R_\infty|, \qquad (4)$$

where $S(\omega)$ is the frequency spectrum of the signal received from the specimen and $S'(\omega)$ is the frequency spectrum of the specular reflection.

Using the above formulation, the experimental form function of the clad rod was recalculated and replotted in Fig. 8. Comparison of the numerical and experimental form functions in Figs. 6b and 8 shows excellent agreement between the two curves through the whole usable bandwidth of the transducer. Moreover, it can be seen that the variations of the experimental form function is smooth and does not show a descending pattern as before.

3. MULTIPLE SCATTERING

When an incident wave impinges on a grating of cylinders, each cylinder generates a scattered field. The scattered field resulting from each cylinder impinges on other cylinders and results in a secondary scattered field. This process continues indefinitely, and is referred to as "multiple scattering of cylinders" and includes the interactions of the cylinders' scattered fields. Therefore, both the properties and geometry of the individual cylinders plus the grating geometry affect the resulting scattered field.

In single scattering, the form function yields three types of information: the resonance frequencies of the elastic cylinder, the profile and width of each resonance, and the smooth background profile.

The procedure and formulation proposed for measuring the form function of a single cylinder can be extended to a grating composed of a number of elastic cylinders. Once again, the smooth background amplitude, $|f^R_\infty|$, is calculated for a single rigid cylinder and used for deconvolving the experimental signal in Eq. (4). The wave interactions between cylinders are not included in $|f^R_\infty|$, but would be included in the experimental signal, $S(\omega)$. In the method proposed for single scattering experiments, we replaced the tungsten fiber signal with its specular reflection. We also replaced the theoretical form function of the tungsten fiber, $|f'_\infty|$, with the numerical form function of a rigid cylinder. The same approach could be used in multiple scattering experiments. In the case of multiple scattering, we can write,

$$|f_\infty| = \left|\frac{S(\omega)}{S'(\omega)}\right| |f^R_\infty|, \qquad (5)$$

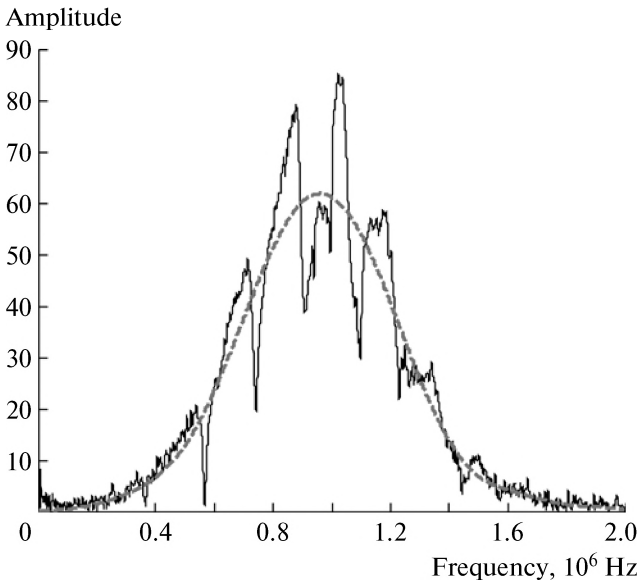

Fig. 9. Frequency spectrum of the signal obtained from a 6.34 mm diameter steel rod (solid line) along with the frequency spectrum of its specular reflection (dashed line).

where $S(\omega)$ is the frequency spectrum of the signal received from the grating, $S'(\omega)$ is the frequency spectrum of the specular reflection of the grid, and $|f_\infty^R|$ is defined as

$$f_\infty^R = \frac{-2}{\sqrt{\pi ika}} \sum_{n=0}^{\infty} \varepsilon_n \frac{J_n'(ka)}{H_n^{(1)'}(ka)} \cos n\phi. \qquad (6)$$

It should be noted that this method is only applicable when all cylinders in the grating have identical diameters.

To demonstrate the validity of the proposed approach, we have tested a grid made from two identical steel rods. Before testing the grid, a reference signal was taken from one of the steel rods. The rod had a diameter of 6.34 mm and was illuminated by a 1 MHz, 0.5 in diameter immersion transducer at normal incidence. The frequency spectra of the received signal and its corresponding specular reflection are shown by solid and dashed lines in Fig. 9, respectively. The resultant form function of the steel rod is shown in Fig. 10 in the frequency range of $4 < ka < 21$.

The configuration of the two rods and transducer is shown in Fig. 11. The center-to-center distance between the two rods is $d_{12} = 30$ mm. The same 1 MHz transducer was used for illuminating the grating in pulse-echo mode. The incident wave was directed along the center-to-center line of the two rods and normal to the z-axis. The frequency spectra of the received signal and its corresponding specular reflection are shown in Fig. 12. The sampling frequency was 50 MS/s in both single and multiple scattering experiments. Using Eq. (5), the measured scattered spectrum of the grating was deconvolved, see Fig. 13. To verify this form function, we compare it with the theoretical form function of the same grating discussed in [27] and shown in Fig. 14. It can be observed that the experimental and theoretical results agree very well.

Comparing the measured form functions of a single steel rod shown in Fig. 10 and a grating of two identical steel rods shown in Fig. 13, we observe that the scattered spectrum obtained from the grating contains

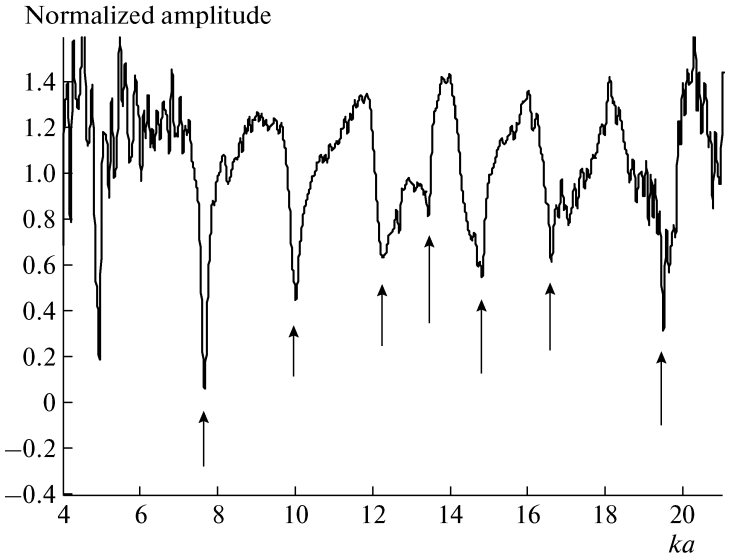

Fig. 10. Measured form function of the 6.34 mm diameter steel rod.

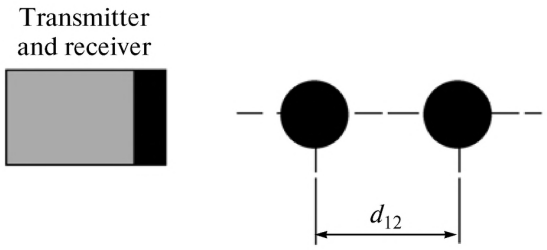

Fig. 11. Configuration of the multiple scattering measurement conducted on a grating of two identical 6.34 mm diameter steel rods separated by 30 mm.

three distinct pieces of information. Two of them pertain to the frequencies and widths of resonances of individual steel rods, as shown by arrows in Figs. 10 and 13. The third piece of information, shown in Fig. 13, features additional oscillations between each two adjacent resonance frequencies. These oscillations could be attributed to reverberation of waves between adjacent rods. This kind of wave interaction is expected and has already been reported in the literature [28].

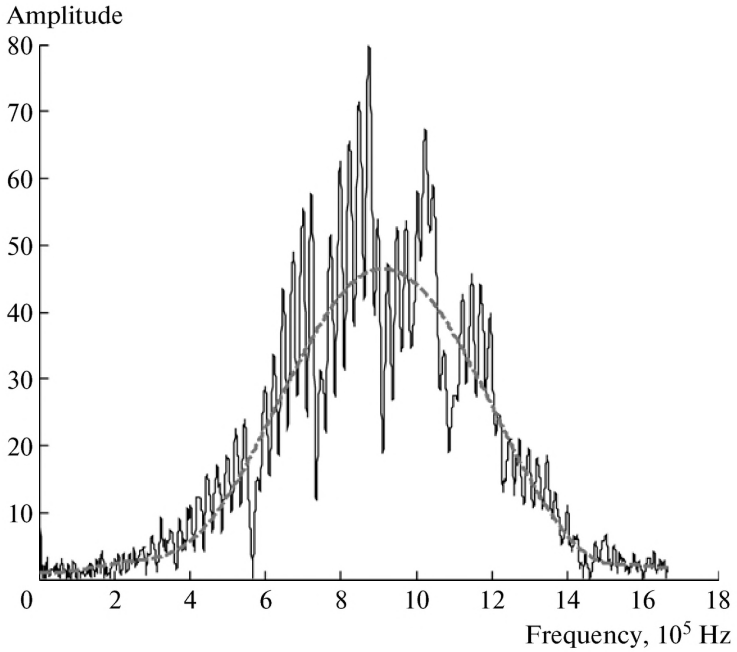

Fig. 12. Frequency spectra of the scattered signal from the grating (solid line) and its specular reflection (dashed line).

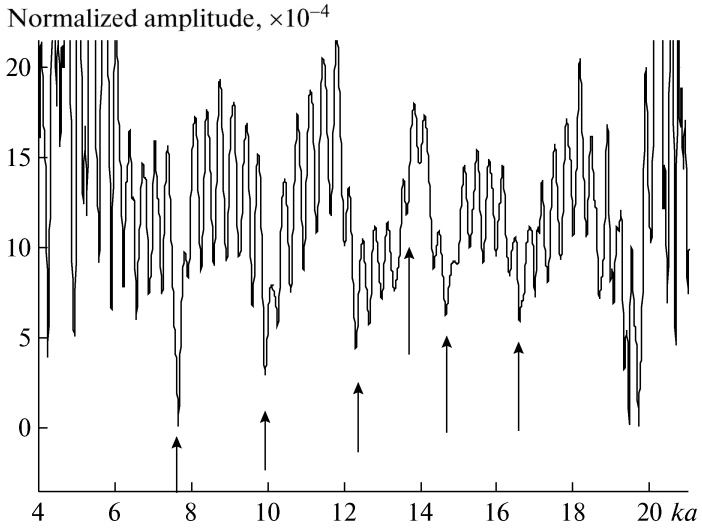

Fig. 13. Measured form function of the grating.

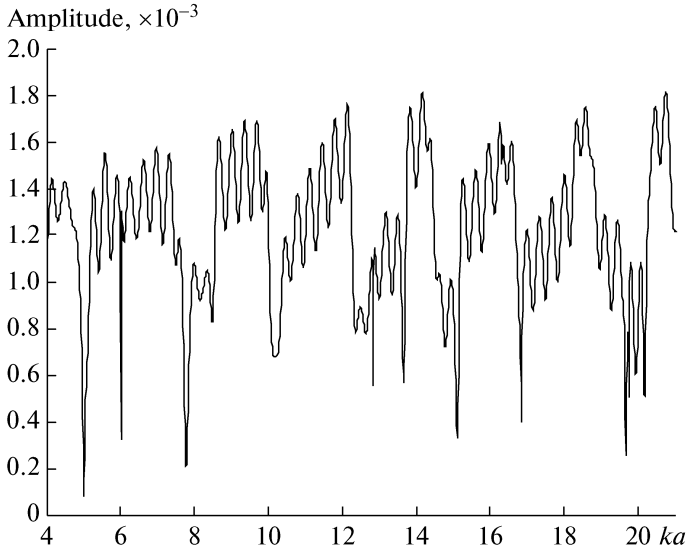

Fig. 14. Calculated form function of the grating.

4. CONCLUSIONS

In this paper, an alternative approach for obtaining the experimental form function of single and multiple cylinders was proposed. In this approach, the specular reflection of the scatterer is extracted from the signal and used for deconvolution purposes. It was shown that there is a mismatch between the frequency spectra of a reference sample such as a tungsten fiber and an elastic rod, when their diameters are different. This difference lowers the accuracy of the deconvolved form function and limits its useful frequency range. Based on the approach used in single scattering experiments, a similar procedure was developed for multiple scattering cases. Experiments were conducted to show that the new approach resolves the existing problems and provides improved accuracy in the measured form functions in both single and multiple scattering experiments.

REFERENCES

1. L. Flax, L. R. Dragonette, and H. Uberall, J. Acoust. Soc. Am. **63**, 723 (1978).
2. H. Uberall, L. R. Dragonette, and L. Flax, J. Acoust. Soc. Am. **61**, 711 (1977).
3. J. W. Dickey and H. Uberall, J. Acoust. Soc. Am. **63**, 319 (1978).
4. L. Flax, G. C. Gaunaurd, and H. Uberall, in *Physical Acoustics*, Ed. by W. P. Mason and R. N. Thurston (Academic, New York, 1981), Vol. 15, pp. 191–293.
5. F. Honarvar, E. Enjilela, and A. N. Sinclair, Acoust. Phys. **55**, 708 (2009).
6. S. M. Hasheminejad and M. Maleki, Acoust. Phys. **54**, 168 (2008).
7. G. Maze, B. Taconet, and J. Ripoche, Phys. Lett. A **84**, 309 (1981).
8. G. Maze and J. Ripoche, Rev. Phys. Appl. **18**, 319 (1983).
9. M. de Billy, J. Acoust. Soc. Am. **79**, 219 (1986).
10. G. Maze and J. Ripoche, in *Acoustic Resonance Scattering*, Ed. by H. Uberall (Gordon and Breach Sci., 1992), pp. 69–103.
11. D. Brill, G. C. Gaunaurd, and H. Uberall, Acoustica **53**, 11 (1983).
12. D. Brill, G. C. Gaunaurd, and H. Uberall, J. Acoust. Soc. Am. **72**, 1067 (1982).
13. F. Honarvar and A. N. Sinclair, J. Acoust. Soc. Am. **102**, 41 (1997).
14. F. Honarvar and A. N. Sinclair, Ultrasonics **36**, 845 (1998).
15. J. Mathieu, P. Schweitzer, and E. Tisserand, Meas. Sci. Technol. **13**, 660 (2002).
16. A. Scipioni, P. Rischette, P. Schweitzer, and J. Mathieu, Meas. Sci. Technol. **20**, 1 (2009).
17. E. Kheddioui, P. Pareige, and J. L. Izbicki, Acoust. Lett. **7**, 157 (1993).
18. S. Lethuillier, P. Pareige, J. L. Izbicki, and J. M. Conoir, in *Proceedings of the 4th European Conference on Underwater Acoustics* (Rome, 1998), p. 837.
19. S. Lethuillier, J. M. Conoir, P. Pareige, and J. L. Izbicki, Ultrasonics **41**, 655 (2003).
20. H. Uberall, *Acoustic Resonance Scattering* (Gordon and Breach Sci., 1992).

21. S. K. Numrich and H. Uberall, in *Physical Acoustics*, Vol. XIX (Academic Press, New York, USA, 1992), Ch. 2, pp. 235–318.

22. F. Honarvar, PhD Dissertation (Univ. of Toronto, 1997).

23. Y. Fan, PhD Dissertation (Univ. of Toronto, 2002).

24. T. Li and M. Ueda, J. Acoust. Soc. Am. **86**, 2363 (1989).

25. J. Fortin, MSc Dissertation (Univ. of Toronto, 2005).

26. L. W. Schmerr and S. J. Song, *Ultrasonic Nondestructive Evaluation Systems, Models and Measurements* (Springer, New York, 2007).

27. S. Sodagar, F. Honarvar, and A. N. Sinclair, "Multiple Scattering of an Obliquely Incident Plane Acoustic Wave from a Grating of Immersed Cylindrical Shells," Applied Acoustics **72**, 1 (2011).

28. J. D. Maynard, Acoust. Today **4** (4) (2008).